Proc. Natl. Sci. Counc. ROC(A)
Vol. 25, No. 4, 2001. pp. 219-231

A Visual Disk Approach for Determining Data Dimensionality in Hyperspectral Imagery

TE-MING TU[*], CHING-HAI LEE[*], CHUNG-SHI CHIANG[*], AND CHIEN-PING CHANG[**]

[*]*Department of Electrical Engineering*
Chung Cheng Institute of Technology
Tao-Yuan, Taiwan, R.O.C.
[**]*Chung-Shan Institute of Science and Technology*
Tao-Yuan, Taiwan, R.O.C.

(Received January 3, 2000; Accepted September 2, 2000)

ABSTRACT

In hyperspectral image analysis, determining a distinct material number is an important task for subsequent classification processes. Identifying the number of distinct materials is essentially the same task as determining the intrinsic dimensionality of the imaging spectrometer data. Minimum noise fraction (MNF) transformation or noise-adjusted principal component analysis (NAPCA) is a highly effective means of determining the inherent dimensionality of image data. However, inaccuracy in the noise estimation degrades the validity of this estimation. To effectively resolve this problem, this work presents a novel visual disk (VD) approach which incorporates the NAPCA method into a transformed Gerschgorin disk (TGD) approach. By means of multiple linear regression, Gerschgorin disks in VD can be formed into two distinct, non-overlapping collections; one for signals and the other for noises. Hence, the number of distinct materials can be visually determined by counting the number of Gerschgorin disks for signals. In addition, the VD approach is evaluated based on both simulated and imaging spectrometer data sets collected by the Airborne Visible Infrared Imaging Spectrometer (AVIRIS). Experimental results demonstrate that the method proposed herein can be used to effectively solve the intrinsic dimensionality problem.

Key Words: noise-adjusted principal components analysis, transformed Gerschgorin disk approach, visual disk approach

I. Introduction

Imaging spectrometry in Earth remote sensing applications largely focuses on determining the identities and abundances of materials in a geographic area of interest. In remote sensing image analysis, the limited spatial resolution of scanners frequently leads to the presence of more than one ground cover type within the instantaneous field of view. Therefore, each spatial coverage pixel often encompasses multiple materials. Under such circumstances, identifying the number of endmembers is equivalent to determining the intrinsic dimensionality of the data rather than the number of clusters of distinct pixels. In multispectral imaging systems, the data dimensionality is often substantially larger than the number of spectral channels. This fact implies that while the intrinsic dimensionality problem is severe for multispectral sensors, only hyperspectral imaging spectrometers have a sufficient number of spectral channels to directly solve this problem. For instance, the NASA Jet Propulsion Laboratory's Airborne Visible/Infrared Imaging Spectrometer (AVIRIS) simultaneously collects 224 spectral bands, each with a 10 nm bandwidth distributed over the 0.4 to 2.4 μm range. However, the Thematic Mapper (TM) used in LANDSAT has only seven spectral bands (Vane and Goetz, 1988).

Conventionally, intrinsic dimensionality is estimated by detecting a gap in singular values. A statistical approach applies hypothesis tests to eigenvalues, which have been derived by means of principal components analysis (PCA) (Anderson, 1984). However, this approach is limited in that it requires a proper set of threshold levels for the dependent sequential test. Moreover, PCA is a linear method, and most noise covariance structures are not known *a priori*. Therefore, using a simple standard PCA in remote sensing is occasionally inadequate. For instance, a previous investigation has demonstrated that when PCA is used in image enhancement (Green *et al.*, 1988), some minor components may contain relevant information rather than only noise or unimportant variance. If these minor components are discarded, the estimation of the intrinsic dimensionality becomes inaccurate. In contrast, when attempting to keep the minor components, the intrinsic dimensionality must be determined by means of image-by-image inspection throughout the entire data space. This makes PCA impractical for application to a hyperspectral image cube.

While addressing similar problems associated with the statistical approach, Wax and Kailath (1985) proposed a novel approach to solving the problem of source number detection. This approach was based on an information theoretical criteria (AIC) (Akaike, 1974) and the minimum description length (MDL) (Rissanen, 1978) criteria. Both the AIC and MDL criteria were adapted to the exponential model-fitting problem. The fact that no subjective judgment is required in these determination processes accounts for why the number of sources can be naturally determined by minimizing the AIC or MDL criterion. However, these two likelihood detectors are derived by means of statistically independent Gaussian random noise with zero mean and the covariance matrix $\boldsymbol{R}_n = \sigma^2\boldsymbol{I}$. Therefore, these techniques can not be directly applied to hyperspectral images since their noise covariance structures are not known in general. In a related work, Wu *et al.* (1995) proposed a transformed Gerschgorin disk approach (TGD) in conjunction with the AIC and MDL criteria to alleviate this problem in the non-Gaussian noise situation and significantly improved the detection performance.

If knowledge or an estimation of the noise covariance is available, the minimum noise fraction (MNF) transformation proposed by Green *et al.* (1988) effectively solves the inherent dimensionality problem. A later investigation by Lee *et al.* (1990) further interpreted this transform as noise-adjusted principal component analysis (NAPCA) with a rapid version proposed by Roger (1990). NAPCA is largely limited in that its noise whitening process requires complete knowledge of the noise structure for the processed data. More specifically, NAPCA must accurately estimate the noise covariance matrix based on the available data. Inaccuracy in the noise estimation degrades NAPCA's ability to calculate the intrinsic dimensionality.

In this work, we present a novel method in two stages to solve the problem of intrinsic dimensionality. The first stage entails as well as involves defining a modified version of the Transformed Gerschgorin Disk approach (MTGD), which incorporates the NAPCA method into TGD. MTGD is advantageous in that it retains the capabilities of both the NAPCA and TGD approaches and simultaneously attempts to determine the intrinsic dimensionality. The second stage, which is now called the Visual Disk (VD) method, is based on multiple linear regression (Anderson, 1984) and functions as a new transform kernel to upgrade the estimation ability and the visualization capability of MTGD. Based on these two stages, the new Gerschgorin disks derived from VD can be formed into two, more distinct signal and noise collections than is the case with TGD and MTGD. Therefore, the number of endmembers can be easily determined by visually counting the number of Gerschgorin disks of signals derived by VD. Experimental results for both simulated and imaging spectrometer data sets collected by the Airborne Visible Infrared Imaging Spectrometer (AVIRIS) demonstrate that the proposed method can be used to accurately determine the intrinsic dimensionality.

II. Problem Formulation

1. Linear Mixture Model for Hyperspectral Images

The linear spectral mixture model is extensively used in remotely sensed imagery to determine and quantify multicomponents. Let $\boldsymbol{r}_i$ be an $l \times 1$ column vector and denote the i-th pixel in a hyperspectral image, where l denotes the number of bands. A linear mixture model for the pixel $\boldsymbol{r}_i$ in a hyperspectral image can be described by (Adams and Smith, 1986)

$$\boldsymbol{r}_i = \boldsymbol{M}\boldsymbol{\alpha}_i + \boldsymbol{n}_i, \tag{1}$$

and its covariance matrix is defined as

$$\boldsymbol{R} = E[\boldsymbol{r}_i\boldsymbol{r}_i^T] = \boldsymbol{M}E(\boldsymbol{\alpha}_i\boldsymbol{\alpha}_i^T)\boldsymbol{M}^T + \boldsymbol{R}_n\ , \tag{2}$$

where $\boldsymbol{M}$ is an $l \times p$ matrix denoted by $(\boldsymbol{m}_1, \boldsymbol{m}_2, \ldots, \boldsymbol{m}_p)$ and $\boldsymbol{m}_i$ is an $l \times 1$ column vector for the spectral signature of the j-th distinct material; p denotes the number of different materials; $\boldsymbol{\alpha}_i$ is a $p \times 1$ column vector given by $(\alpha_1, \alpha_2, \ldots, \alpha_p)^T$, where α_j represents the fraction of the j-th signature present in $\boldsymbol{r}_i$; $\boldsymbol{n}_i$ is an $l \times 1$ column vector for the combined noise, which is assumed to be a wide sense stationary Gaussian process with zero mean and covariance matrix $\boldsymbol{R}_n$.

Equivalently, Eq. (1) can be expressed as a standard signal model:

$$\boldsymbol{r}_i = \boldsymbol{s}_i + \boldsymbol{n}_i. \tag{3}$$

When the noise $\boldsymbol{n}$ and signal $\boldsymbol{s}$ are assumed to be uncorrelated, the covariance matrix $\boldsymbol{R}$ in Eq. (2) can be represented as follows:

$$\boldsymbol{R} = \boldsymbol{R}_s + \boldsymbol{R}_n. \tag{4}$$

Notably, the covariance matrix $\boldsymbol{R}$ is an $l \times l$ matrix. Meanwhile, the noise covariance matrix $\boldsymbol{R}_n$ is of full rank l, and the signal covariance matrix $\boldsymbol{R}_s = \boldsymbol{M}E[\boldsymbol{\alpha}\boldsymbol{\alpha}^T]\boldsymbol{M}^T$ is of rank p. Therefore, the inherent dimensionality problem attempts to determine the value of p based on a given $\boldsymbol{R}$.

However, our problem largely focuses on accurately finding the inherent dimensionality in a low SNR situation, where some materials may have a low probability of occurrence within the scene. This low probability implies that these materials only appear in a small number of pixels or mixed pixels. When the signal energy of materials is smaller than the noise energy in the entire image, the intrinsic dimensionality is generally underestimated. Restated, the intrinsic dimensionality may be underestimated when some eigenvalues in the estimated signal-subspace are extremely close to an increasing, estimated noise variance.

2. Determining the Intrinsic Dimensionality by Means of PCA

PCA is perhaps the simplest estimation scheme for application to the inherent dimensionality problem (Anderson, 1984). The PCA technique, also known as the Karhunen-Loeve transform, is a decorrelation scheme used to compress and interpret data. In addition, the gap in the distribution of singular values is the primary source used to determine the inherent dimensionality by PCA.

PCA can be initiated by assuming that the covariance matrix $\boldsymbol{R}$ expressed in Eq. (4) is nonnegative and can be decomposed as

$$\boldsymbol{R} = \boldsymbol{\Phi}\boldsymbol{\Lambda}\boldsymbol{\Phi}^T = [\boldsymbol{\Phi}_s \boldsymbol{\Phi}_n]\begin{bmatrix} \boldsymbol{\Lambda}_s & 0 \\ 0 & \boldsymbol{\Lambda}_n \end{bmatrix}[\boldsymbol{\Phi}_s \boldsymbol{\Phi}_n]^T, \tag{5}$$

where $\boldsymbol{\Phi}$ is a matrix whose columns consist of all the distinct eigenvectors of $\boldsymbol{R}$. This matrix can be further partitioned into two parts, i.e., $\boldsymbol{\Phi}_s$ and $\boldsymbol{\Phi}_n$, corresponding to signal $\boldsymbol{s}$ and noise $\boldsymbol{n}$, respectively.

According to Eq. (5), if the noise statistics are assumed to have a Gaussian distribution with zero mean and covariance matrix $\boldsymbol{R}_n = \sigma^2\boldsymbol{I}$, then $\boldsymbol{\Lambda}_s = diag(\lambda_1, \lambda_2, \ldots, \lambda_p)$ with $\{\lambda_i\}_{i=1}^{p} = \lambda_i' + \sigma^2$ and $\boldsymbol{\Lambda}_n = diag(\lambda_{p+1}, \lambda_{p+2}, \ldots, \lambda_l)$ with $\{\lambda_i\}_{i=p+1}^{l} = \sigma^2$ are eigenvalues corresponding to $\boldsymbol{\Phi}_s$ and $\boldsymbol{\Phi}_n$, respectively. Based on the distribution of singular values, the dimensionality (p) can be estimated because a gap is expected to exist between the p largest eigenvalues and the remaining noise eigenvalues. Unfortunately, the knowledge of $\boldsymbol{R}_n$ is generally unavailable in practice, and its statistical property must be obtained from the given data. Hence, determining the data dimensionality becomes tricky, particularly for a low SNR situation, where some eigenvalues in the estimated signal-subspace are nearly equal to the estimated noise variance. A well-known statistical multiple-hypothesis testing procedure, the Lawley-Bartlett test (Anderson, 1984), seems to be useful here. However, this test is limited in a practical sense in that it requires a proper set of threshold levels for the dependent sequential test. A previous investigation (Anderson, 1984) demonstrated that this test function is essentially the generalized likelihood ratio test, implying that thresholds of this test do not ensure that all minor components consist of noises or unimportant variance only. Therefore, the PCA approach can not be directly applied to hyperspectral images to determine their intrinsic dimensionality.

3. Determining the Intrinsic Dimensionality by Means of NAPCA

In PCA, a transformed band with small variance does not imply poor image quality; it may be a high SNR band in which others are of large variance or are low SNR bands. To address this problem, Green *et al*. (1988) proposed a minimum noise fraction (MNF) transformation to arrange principal components in a descending order of the image quality rather than of the variance. Subsequent investigations by Lee *et al*. (1990) and Roger (1990) reinterpreted this transform as NAPCA. The NAPCA approach can be regarded as a two-stage, cascaded principal component transformation with a diagonalization procedure (Fukanaga, 1990) used to achieve the maximum signal-noise-ratio (MSNR), i.e., to derive a matrix $\boldsymbol{A}$ such that

$$\max_{A} \frac{\boldsymbol{A}^T\boldsymbol{R}\boldsymbol{A}}{\boldsymbol{A}^T\boldsymbol{R}_n\boldsymbol{A}} = \max_{A} \frac{\boldsymbol{A}^T\boldsymbol{R}_s\boldsymbol{A}}{\boldsymbol{A}^T\boldsymbol{R}_n\boldsymbol{A}} + 1 \tag{6a}$$

(due to Eq. (4)) or, equivalently,

$$\boldsymbol{A}^T\boldsymbol{R}\boldsymbol{A} = \boldsymbol{\Lambda} \tag{6b}$$

and

$$\boldsymbol{A}^T\boldsymbol{R}_n\boldsymbol{A} = \boldsymbol{I}. \tag{6c}$$

To obtain the desired transformation in Eq. (6), a whitening process can be designed to simultaneously transform $\boldsymbol{R}_n$ and $\boldsymbol{R}$. Restated,

$$\boldsymbol{W}^T\boldsymbol{R}_n\boldsymbol{W} = \boldsymbol{I} \tag{7a}$$

and

$$\boldsymbol{W}^T\boldsymbol{R}\boldsymbol{W} = \boldsymbol{R}_{adj}, \tag{7b}$$

where $\boldsymbol{W} = \boldsymbol{\Phi}_n\boldsymbol{\Lambda}_n^{-1/2}$ denotes the transformation matrix, and $\boldsymbol{\Lambda}_n$ and $\boldsymbol{\Phi}_n$ represent eigenvalue and eigenvector matrices of $\boldsymbol{R}_n$, respectively. The adjusted covariance matrix $\boldsymbol{R}_{adj}$ is, in general, not a diagonal but a symmetric matrix.

Using the eigenvectors of $\boldsymbol{R}_{adj}$, i.e., $\boldsymbol{\Phi}_{adj}$, as the basis for the second transformation leads to

$$\boldsymbol{\Phi}_{adj}^T\boldsymbol{I}\,\boldsymbol{\Phi}_{adj} = \boldsymbol{I} \text{ (due to } \boldsymbol{\Phi}_{adj}^T\boldsymbol{\Phi}_{adj} = \boldsymbol{I}) \tag{8a}$$

and

$$\boldsymbol{\Phi}_{adj}^T\boldsymbol{R}_{adj}\boldsymbol{\Phi}_{adj} = \boldsymbol{\Lambda}_{adj}. \tag{8b}$$

Consequently, the desired NAPCA transform can be derived by using

$$\boldsymbol{A} = \boldsymbol{\Phi}_n\boldsymbol{\Lambda}_n^{-1/2}\boldsymbol{\Phi}_{adj}. \tag{9}$$

The subsequent transformed covariance matrix is, then, expressed as

$$\boldsymbol{R}_{Y,\ NAPCA}$$

$$= \boldsymbol{A}^T\boldsymbol{R}\boldsymbol{A}$$

$$= \begin{bmatrix} \bar{\lambda}_1 & 0 & \cdots & 0 & 0 & \cdots & 0 \\ & & & & \vdots & & \\ 0 & 0 & \cdots & \bar{\lambda}_p & 0 & \cdots & 0 \\ 0 & 0 & \cdots & 0 & \bar{\lambda}_{p+1} & \cdots & 0 \\ & & & & \vdots & & \\ 0 & 0 & \cdots & 0 & 0 & \cdots & \bar{\lambda}_l \end{bmatrix}. \tag{10}$$

Consider a situation in which the noise covariance matrix $\boldsymbol{R}_n$ is accurately estimated based on the data. This allows us to partition the transformed data space into two portions: one consists of eigenvalues larger than one and the other eigenvalues of unity. This observation implies that $\{\bar{\lambda}_i\}_{i=1}^{p} = \dot{\lambda}_i + 1$ and $\{\bar{\lambda}_i\}_{i=p+1}^{l} = 1$, where $\{\dot{\lambda}_i\}_{i=1}^{p}$ represents the associated eigenvalues for the signal covariance matrix $\boldsymbol{R}_s$. Under such circumstances, the inherent dimensionality of the data can be determined by examining the number of eigenvalues larger than unity. However, this algorithm does not, in general, function properly, particularly in remote sensing images, owing to a variety of unknown noises and unexpected interferences from the atmosphere. If the condition that noise statistics be estimated is not of concern, then eigenvalues for noises are not simply unity or near-unity, but increases due to the incompleteness of the estimated noise statistics. Actually, it is implied that the more incomplete the noise statistics, the larger the noise eigenvalues. Consequently, the intrinsic dimensionality may be underestimated when some eigenvalues in the estimated signal-subspace are very near the increased estimated noise variance in a low SNR situation.

III. The Gerschgorin Disk Theorem and Its Transformation

The Gerschgorin disk theorem (Alan, 1977) and Wu's related transformation approach (Wu *et al.*, 1995) are reviewed in the following:

1. Gerschgorin Disk Theorem

If $\boldsymbol{A}$ is an $l \times l$ real or complex matrix, a_{jk} denotes the elements of $\boldsymbol{A}$, j, $k = 1, \ldots, l$, and

$$\rho_j = \sum_{\substack{k=1 \\ k \neq j}}^{l} \left| a_{jk} \right|, \tag{11}$$

then each eigenvalue of $\boldsymbol{A}$ lies in one of the disks in the complex plane

$$D_j = \{z\colon |z - a_{jj}| \leq \rho_j\},\ \ j = 1, 2, \ldots, l, \tag{12}$$

where a_{jj} and ρ_j are called the Gerschgorin center and Gerschgorin radius, respectively. The proof of this theorem given by Alan (1977) demonstrates not only that each eigenvalue of $\boldsymbol{A}$ must lie in a Gerschgorin disk, but also that if the j-th component of an eigenvector is maximum, the corresponding eigenvalue must lie in the j-th disk.

According to Wu *et al.* (1995), the Gerschgorin disks of the covariance matrix (*e.g.*, $\boldsymbol{R}$) provide no assistance in determining the number of sources because the Gerschgorin disks for this matrix could tightly overlap when its eigenvalues are spread over a large range. Based on this fact, the Gerschgorin disks for the original covariance matrix are not facilitative in determining the intrinsic dimensionality in a hyperspectral image either.

2. Wu's Transformation Approach

To make Gerschgorin's disk theorem effective, Wu *et al.* (1995) proposed a proper unitary transformation, called the transformed Gerschgorin disk (TGD) approach, to rotate the sample covariance matrix. The designed unitary transformation has the ability to render the noise Gerschgorin disks as small and as remote from the signal Gerschgorin disks as possible. After this transformation, Gerschgorin disks can be divided into two collections for signals and noises, respectively. The signal collection has a larger Gerschgorin radii and contains exactly p largest signal eigenvalues while the noise collection has a small Gerschgorin radii and contains the remaining noise eigenvalues. In this manner, the number of endmembers can be determined by counting the number of signal Gerschgorin disks.

Following the notation defined in Eq. (4), where $\boldsymbol{R}$ denotes the covariance matrix of $\boldsymbol{r}$, the unitary transform starts by rewriting the covariance matrix $\boldsymbol{R}$ into a partition form as follows:

$$\boldsymbol{R} = \begin{bmatrix} \boldsymbol{C} & \underline{\boldsymbol{c}}_l \\ \underline{\boldsymbol{c}}_l^T & c_{l,l} \end{bmatrix}, \tag{13}$$

where $\underline{\boldsymbol{c}}_l^T = [c_{l,1}, c_{l,2}, \ldots, c_{l,l-1}]$ and $\boldsymbol{C}$ is an $(l-1) \times (l-1)$ leading principal submatrix of $\boldsymbol{R}$ obtained by deleting the last row and column of this covariance matrix. More specifically, $\boldsymbol{C}$ can be regarded as the reduced covariance matrix obtained by removing the l-th sensor from the imaging system but keeping all other $(l-1)$ sensors. Since $\boldsymbol{C}$ is symmetric and nonnegative, it can be decomposed by means of its eigenstructure as

$$\boldsymbol{C} = \boldsymbol{Q}_c \boldsymbol{\Lambda}_c \boldsymbol{Q}_c^T, \tag{14}$$

where elements of the diagonal matrix $\boldsymbol{\Lambda}_c$ are eigenvalues of the reduced covariance matrix arranged in descending order, i.e., $\boldsymbol{\Lambda}_c = diag(\hat{\lambda}_1, \hat{\lambda}_2, \ldots, \hat{\lambda}_{l-1})$ with $\hat{\lambda}_1 \geq \hat{\lambda}_2, \ldots, \geq \hat{\lambda}_{l-1}$. $\boldsymbol{Q_c} = (\boldsymbol{q}_1, \boldsymbol{q}_2, \ldots, \boldsymbol{q}_p, \ldots, \boldsymbol{q}_{l-1})$ is an $(l-1) \times (l-1)$ unitary matrix whose columns are the corresponding orthonormal eigenvectors of $\boldsymbol{C}$.

Now, an $l \times l$ unitary transformation matrix $\boldsymbol{Q}$ is constructed so as to rotate the covariance matrix $\boldsymbol{R}$ given in Eq. (13). This unitary matrix is defined by

$$\boldsymbol{Q} = \begin{bmatrix} \boldsymbol{Q}_c & \underline{\boldsymbol{0}} \\ \underline{\boldsymbol{0}} & 1 \end{bmatrix}. \tag{15}$$

The transformed covariance matrix becomes

$$\boldsymbol{R}_{Y,TGD} = \boldsymbol{Q}^T\boldsymbol{R}\boldsymbol{Q} = \begin{bmatrix} \boldsymbol{Q}_c^T\boldsymbol{C}\boldsymbol{Q}_c & \boldsymbol{Q}_c^T\underline{\boldsymbol{c}}_l \\ \underline{\boldsymbol{c}}_l^T\boldsymbol{Q}_c & c_{l,l} \end{bmatrix}$$

$$= \begin{bmatrix} \hat{\lambda}_1 & 0 & \cdots & 0 & \gamma_1 \\ 0 & \hat{\lambda}_2 & \cdots & 0 & \gamma_2 \\ & & \vdots & & \\ 0 & 0 & \cdots & \hat{\lambda}_{l-1} & \gamma_{l-1} \\ \gamma_1 & \gamma_2 & \cdots & \gamma_{l-1} & c_{l,l} \end{bmatrix}, \tag{16}$$

where $\hat{\lambda}_i$ and $\gamma_i = \boldsymbol{q}_i^T\underline{\boldsymbol{c}}_l$ $(i = 1, 2, \ldots, l-1)$ are the i-th transformed Gerschgorin center and Gerschgorin radius, respectively. When the noise statistics have a Gaussian distribution with zero mean and covariance matrix $\boldsymbol{R}_n = \sigma^2\boldsymbol{I}$, Eq. (16) results in

$$\boldsymbol{R}_{Y,TGD} = \begin{bmatrix} \hat{\lambda}_1 & \cdots & 0 & 0 & \cdots & 0 & \gamma_1 \\ & & & \vdots & & & \\ 0 & \cdots & \hat{\lambda}_p & 0 & \cdots & 0 & \gamma_p \\ 0 & \cdots & 0 & \sigma^2 & \cdots & 0 & 0 \\ & & & \vdots & & & \\ 0 & \cdots & & & \cdots & \sigma^2 & 0 \\ \gamma_1 & \cdots & \gamma_p & 0 & \cdots & 0 & c_{l,l} \end{bmatrix}. \tag{17}$$

Comparing Eq. (17) with Eq. (16) reveals that all of the values for γ_i, $i = p + 1, p + 2, \ldots, l - 1$, are equal to zero because the noise eigenvectors $\boldsymbol{q}_i$ are orthogonal to the signal covariance energies $\underline{\boldsymbol{c}}_l$. Restated, disks with zero Gerschgorin radii can be regarded as the collection of noise Gerschgorin disks while the remaining disks containing non-zero Gerschgorin radii and larger center values (i.e., $\hat{\lambda}_1, \hat{\lambda}_2, ..., \hat{\lambda}_p$) can be regarded as the signal Gerschgorin disks. The notion of using the TGD to determine the intrinsic dimensionality arises from the phenomenon that noise disks with zero Gerschgorin radii can be easily separated from signal disks. Hence, the number of endmembers can be visually determined by counting the number of signal Gerschgorin disks. However, as in PCA and NAPCA, noise eigenvectors $(\boldsymbol{q}_i)_{i=p+1}^{l-1}$ may not be orthogonal to $\underline{\boldsymbol{c}}_l$ when the structure of the noise is not known *a priori*. This phenomenon again implies that $\boldsymbol{R}_n \neq \sigma^2\boldsymbol{I}$ and noise disks do not have zero Gerschgorin radii. At this point, the signal and noise disks may overlap when the SNR is low.

IV. The Visual Disk Approach

1. Incorporating NAPCA into TGD

The above discussion clearly indicates that the NAPCA and TGD approaches have their distinctive strengths. A strategy for simultaneously retaining the merits of both the NAPCA and TGD approaches involves putting these noise Gerschgorin centers in perspective by incorporating the NAPCA approach in order to produce smaller Gerschgorin values. To implement this strategy, the $\boldsymbol{R}$ in Eq. (13) should be replaced by $\boldsymbol{R}_{adj}$, the noise-adjusted covariance matrix in Eq. (7). Proceeding in the same manner as in Eqs. (13) – (15) leads to

$$\boldsymbol{R}_{adj} = \begin{bmatrix} \tilde{\boldsymbol{C}} & \tilde{\underline{\boldsymbol{c}}}_l \\ \tilde{\underline{\boldsymbol{c}}}_l^T & \tilde{c}_{l,l} \end{bmatrix} \tag{18a}$$

with the same eigenstructure as in Eq. (14),

$$\tilde{\boldsymbol{C}} = \tilde{\boldsymbol{Q}}_c\tilde{\boldsymbol{\Lambda}}_c\tilde{\boldsymbol{Q}}_c^T, \tag{18b}$$

and the same transform kernel as in Eq. (15),

$$\tilde{\boldsymbol{Q}} = \begin{bmatrix} \tilde{\boldsymbol{Q}}_c & \underline{\boldsymbol{0}} \\ \underline{\boldsymbol{0}} & 1 \end{bmatrix}. \tag{18c}$$

By using the transform structure of the TGD method, a modified TGD (MTGD) transformation method which has the strengths of both the NAPCA and TGD approaches can, therefore, be constructed as follows:

$$\boldsymbol{R}_{Y,MTGD}$$

$$= \tilde{\boldsymbol{Q}}^T E(\boldsymbol{r}_{adj}\boldsymbol{r}_{adj}^T)\tilde{\boldsymbol{Q}} = \tilde{\boldsymbol{Q}}^T\boldsymbol{R}_{adj}\tilde{\boldsymbol{Q}} = E(\boldsymbol{y}\boldsymbol{y}^T)$$

$$= \begin{bmatrix} \tilde{\lambda}_1 & \cdots & 0 & 0 & \cdots & 0 & \tilde{\gamma}_1 \\ & & & & \vdots & & \\ 0 & \cdots & \tilde{\lambda}_p & 0 & \cdots & 0 & \tilde{\gamma}_p \\ 0 & \cdots & 0 & \tilde{\lambda}_{p+1}(\approx 1) & \cdots & 0 & \tilde{\gamma}_{p+1}(\approx 0) \\ & & & & \vdots & & \\ 0 & \cdots & 0 & 0 & \cdots & \tilde{\lambda}_{l-1}(\approx 1) & \tilde{\gamma}_{l-1}(\approx 0) \\ \tilde{\gamma}_1 & \cdots & \tilde{\gamma}_p & \tilde{\gamma}_{p+1} & \cdots & \tilde{\gamma}_{l-1} & \tilde{c}_{l,l} \end{bmatrix}, \tag{19a}$$

$$y = \tilde{Q}^T r_{adj}\ , \tag{19b}$$

where r_{adj} denotes the noise-adjusted observation vector with a noise-adjusted covariance matrix, i.e., R_{adj}.

Comparing Eq. (19a) with Eq. (17) reveals that the centers of the noise Gerschgorin disks, i.e., $(\hat{\lambda}_1)_{i=p+1}^{l-1}$ versus $(\tilde{\lambda}_i)_{i=p+1}^{l-1}$, are reduced from σ^2 to unity. Restated, the subsequent noise disk collection obtained by MTGD is more remote from the signal disk collection obtained by TGD. Therefore, MTGD is obviously more appropriate for determining the intrinsic dimensionality than is TGD. Moreover, when the noise statistics can not be completely estimated, the NAPCA method fails in a low SNR situation; however, MTGD may not. Under such circumstances, determining the intrinsic dimensionality should depend on the connection conditions of the Gerschgorin disks. Such a situation implies that MTGD will be underestimated if a few signal Gerschgorin disks with small eigenvalues overlap with the largest noise Gerschgorin disk. In contrast, MTGD works successfully if these two collections do not overlap. Consequently, the Gerschgorin radius heavily influences the determination of the intrinsic dimensionality. Hence, the method capable of reducing the size of the radii of Gerschgorin disks should help solve this problem.

2. The Proposed VD

In light of these requirements, an effective intrinsic dimensionality estimation method must select a proper transformation having the ability to reduce the size of the radii of Gerschgorin disks as much as possible and to make noisy Gerschgorin disks as remote from signal Gerschgorin disks as possible. In this section, we will present a novel transform kernel based on the concept of multiple linear regression to improve MTGD.

Similar to the partition structure used in the MTGD method, a noise-adjusted observation vector r_{adj} can be partitioned as $[\underline{r}, r_l]^T$, where $\underline{r} = [r_1, r_2, \ldots, r_{l-1}]^T$. According to the definition of multiple linear regression (Anderson, 1984), the maximum correlation between r_l and the linear combination $\beta^T \underline{r}$ is called the multiple correlation coefficient between r_l and the linear combination $\underline{r}$, which is defined as

$$\rho_{r_l, \beta^T \underline{r}} = \frac{\sqrt{\underline{\tilde{c}}_l^T \tilde{C}^{-1} \underline{\tilde{c}}_l}}{\sqrt{\tilde{c}_{l,l}}}\ , \tag{20}$$

where the multiple correlation coefficient, $\rho_{r_l, \beta^T \underline{r}}$, lies in the range of [0, 1] but not [–1, 1]. β represents the partial regression coefficients and $\beta = C^{-1}\underline{c}_l$.

An important property of multiple linear regression (Anderson, 1984) which is useful in our discussions is as follows: For every vector α,

$$corr(r_l, \beta^T \underline{r}) \geq corr(r_l, \alpha^T \underline{r}). \tag{21}$$

According to the definition of multiple linear regression, the correlation between r_l and the linear combination $\alpha^T \underline{r}$ can be derived as

$$\rho_{r_l, \alpha^T \underline{r}} = \frac{\alpha^T \underline{\tilde{c}}_l}{\sqrt{\tilde{c}_{l,l}}\sqrt{\alpha^T \tilde{C} \alpha}}\ . \tag{22}$$

A situation in which the eigenvectors $\tilde{Q}_c = (\tilde{q}_1, \tilde{q}_2, \ldots, \tilde{q}_p, \ldots, \tilde{q}_{l-1})$ defined in Eq. (18b) are used to replace α in Eq. (22) leads to

$$\rho_{r_l, \tilde{q}_i^T \underline{r}} = \frac{\tilde{q}_i^T \underline{\tilde{c}}_l}{\sqrt{\tilde{c}_{l,l}}\sqrt{\tilde{q}_i^T \tilde{C} \tilde{q}_i}} = \frac{\tilde{q}_i^T \underline{\tilde{c}}_l}{\sqrt{\tilde{c}_{l,l}}\sqrt{\tilde{\lambda}_i}} = \frac{\tilde{\gamma}_i}{\sqrt{\tilde{c}_{l,l}}\sqrt{\tilde{\lambda}_i}}\ ,$$

$$i = 1, 2, \ldots, l-1. \tag{23}$$

Recalling Eq. (19), note that both the transformed Gerschgorin radius $\tilde{\gamma}_i = \tilde{q}_i^T \underline{\tilde{c}}_l$ in Eq. (19) and $\rho_{r_l, \tilde{q}_i^T \underline{r}}$ in Eq. (23) have the same form but different normalized factors. Nevertheless, $\rho_{r_l, \tilde{q}_i^T \underline{r}}$ is the standard correlation coefficient, and it lies in the range [–1,1] but not [0,1].

From the point of view of signal energy, the vector $\underline{\tilde{c}}_l$ can be regarded as a collection of the redundancy energies between the last band numbered l and the first $(l-1)$ bands. Thus, the radius $\tilde{\gamma}_i$ ($\tilde{\gamma}_i = \tilde{q}_i^T \underline{\tilde{c}}_l$) for a transformed covariance is the magnitude of the projection from $\tilde{q}_i$ to $\underline{\tilde{c}}_l$, which can also be interpreted as a transformed redundancy. However, although eigenvectors $(\tilde{q}_i)_{i=1}^{l-1}$ are orthonormal, it is not guaranteed that no overlapping will occur between two adjacent transformed redundancies. This observation implies that $\tilde{\gamma}_i = \tilde{q}_i^T \underline{\tilde{c}}_l$ and $\tilde{\gamma}_{i+1} = \tilde{q}_{i+1}^T \underline{\tilde{c}}_l$ could overlap each other. Hence, a limitation of using the transformed covariance as the Gerschgorin radius is that the smallest signal Gerschgorin disk may overlap with the subsequent noise Gerschgorin disks.

In contrast to the transformed covariance $\tilde{\gamma}_i$, the correlation coefficient $\rho_{r_l, \tilde{q}_i^T \underline{r}}$ is a correlation relationship between r_l and the transformed coefficients y. According to Eq. (19), the noise-adjusted observation vector r_{adj} is partitioned as $[\underline{r}, r_l]^T$, where $\underline{r} = [r_1, r_2, \ldots, r_{l-1}]^T$. The pixel r_l represents the signal received from the l-th sensor and can be expressed in standard form as $r_l = s_l + n_l$. Actually, the noise energy must be overwhelmingly less than the signal energy in this single band for a very clear image. Therefore, when $\tilde{q}_i$ is an eigenvector of a signal, the correlation coefficient $\rho_{r_l, \tilde{q}_i^T \underline{r}}$ is not zero. $\rho_{r_l, \tilde{q}_i^T \underline{r}}$ can be regarded as a predication degree by using the transformed coefficient y_i ($y_i = \tilde{q}_i^T \underline{r}$) to accurately predict the final band signal r_l. This implies that the higher this correlation coefficient, the better the predication. If $\tilde{q}_i$ is a noise eigenvector, then $\rho_{r_l, \tilde{q}_i^T \underline{r}}$ is near-zero because the noise eigenvector is orthogonal to the signal r_l. Based on this fact, by using $\rho_{r_l, \tilde{q}_i^T \underline{r}}$ to replace $\tilde{\gamma}_i$ as a new Gerschgorin radius, the radii size of Gerschgorin disks can be reduced until it is as small as possible, and the noisy Gerschgorin disks can be kept as far from the signal Gerschgorin disks as possible.

Consequently, the correlation coefficient $\rho_{r_l,\tilde{q}_i^T\underline{r}}$ is more likely to be a Gerschgorin radius than the transformed covariance $\tilde{\gamma}_i$. So that $\rho_{r_l,\tilde{q}_i^T\underline{r}}$ can be used to replace $\tilde{\gamma}_i$ in Eq. (19a), a nonsingular matrix is defined as follows:

$$\boldsymbol{D} = diag(\sqrt{\tilde{\lambda}_1}\sqrt{\tilde{c}_{l,l}}, \sqrt{\tilde{\lambda}_2}\sqrt{\tilde{c}_{l,l}}, ..., \sqrt{\tilde{\lambda}_{l-1}}\sqrt{\tilde{c}_{l,l}}, 1)$$

$$= diag(\kappa_1, \kappa_2, \ldots, \kappa_{l-1}, 1), \quad \textbf{(24)}$$

where $\kappa_i = \sqrt{\tilde{\lambda}_i}\sqrt{\tilde{c}_{l,l}}$, $i = 1, 2, \ldots, l-1$. Inserting Eq. (24) into Eq. (19a) results in a form similar to that of Eq. (19a). Then, the VD approach can be derived as

$$\boldsymbol{Y} = \boldsymbol{D}^{-1}\tilde{\boldsymbol{Q}}^T\boldsymbol{R}_{adj}\tilde{\boldsymbol{Q}}\boldsymbol{D} = \begin{bmatrix} \tilde{\lambda}_1 & \cdots & 0 & 0 & \cdots & 0 & \tilde{\gamma}_1/\kappa_1\ (<1) \\ & & & & \vdots & & \\ 0 & \cdots & \tilde{\lambda}_p & 0 & \cdots & 0 & \tilde{\gamma}_p/\kappa_p\ (<1) \\ 0 & \cdots & 0 & \tilde{\lambda}_{p+1}\ (\approx 1) & \cdots & 0 & \tilde{\gamma}_{p+1}/\kappa_{p+1}\ (\approx 0) \\ & & & & \vdots & & \\ 0 & \cdots & 0 & 0 & \cdots & \tilde{\lambda}_{l-1}\ (\approx 1) & \tilde{\gamma}_{l-1}/\kappa_{l-1}\ (\approx 0) \\ \tilde{\gamma}_1\cdot\kappa_1 & \cdots & \tilde{\gamma}_p\cdot\kappa_p & \tilde{\gamma}_{p+1}\cdot\kappa_{p+1} & \cdots & \tilde{\gamma}_{l-1}\cdot\kappa_{l-1} & \tilde{c}_{l,l} \end{bmatrix}. \quad \textbf{(25)}$$

Hence, the first $(l-1)$ Gerschgorin disks possess the new Gerschgorin radii:

$$\tilde{\gamma}'_i = \frac{\tilde{\gamma}_i}{\kappa_i} = \frac{\tilde{\boldsymbol{q}}_i^T\tilde{\boldsymbol{c}}_l}{\sqrt{\tilde{\lambda}_i}\sqrt{\tilde{c}_{l,l}}}, \ i = 1, ..., l-1. \quad \textbf{(26)}$$

3. Implementation Considerations

In practice, the probability distributions governing $\boldsymbol{r}$ are not known. Consequently, the statistical covariance matrices used in the above derivations are unavailable but must be estimated by means of the sample covariance matrix $\boldsymbol{R} = \frac{1}{N}\sum_{i=1}^{N}\boldsymbol{r}_i\boldsymbol{r}_i^T$, where $\{\boldsymbol{r}_i\}_{i=1}^N$ denotes a sequence of N observation vectors. The VD procedure is, then, executed as follows.

(1) First, the noise covariance matrix $\boldsymbol{R}_n$ is estimated based on the hyperspectral image cube. The simplest method for making such an estimation is the "shift difference" approach, which is a sub-function available in the commercial package ENVI (ENVI, 1997). This approach assumes that each pixel contains both signal and noise; therefore, adjacent pixels contain the same signal but different noise. The "shift difference" method is performed on the data by differencing adjacent pixels to the right and above each pixel and averaging the results to obtain the "noise" value that should be assigned to the pixel being processed. However, the optimal noise estimate is derived from the shift-difference statistics of a homogeneous area rather than the entire image.

(2) Implement the whitening process of NAPCA in Eq. (7) to obtain $\boldsymbol{R}_{adj}$. Here, the second stage in NAPCA, i.e., the standard PCA, is not necessary.

(3) Calculate the unitary and nonsingular matrices by means of Eqs. (18c) and (24), respectively.

(4) When $\boldsymbol{D}$, $\tilde{\boldsymbol{Q}}$, and $\boldsymbol{R}_{adj}$ are obtained, the VD approach can be implemented by using Eq. (25). The first $l-1$ Gerschgorin disks can then be plotted.

(5) Determine the number of endmembers by counting the number of signal Gerschgorin disks. After this is done, the task is completed.

V. Experimental Results

The analysis performed in this study included two data cubes acquired over the Cuprite, Nevada, and the Lunar Crater Volcanic Field (LCVF), Northern Nye County, Nevada, in 1992 using the NASA/JPL AVIRIS instrument. Experiment for each location included a simulator and actual detection data. Four methods were evaluated in the experiments: (1) the PCA transform given by Eq. (5), (2) the NAPCA transform given by Eq. (10), (3) the MTGD transform given by Eq. (19a) and (4) the proposed VD transform given by Eq. (25).

Experiment 1. The data set used in the first experiment was a subsection of the Cuprite image, which is a 200 × 200 pixel scene. Figure 1 depicts the 0.752 μm band of the image. Since bands corresponding to the water absorption regions and the low SNR bands had no useful energy, they were removed prior to processing, which left 192 bands in this study. This area has been extensively studied using field measurements (Swayze *et al.*, 1992), where the "alphabet" symbols denote the regions of pure materials, which have been found to contain six significant materials: playa, kaolinite, alunite, silica, buddingtonite, and varnished tuff. Figure 2 displays the radiance spectra for

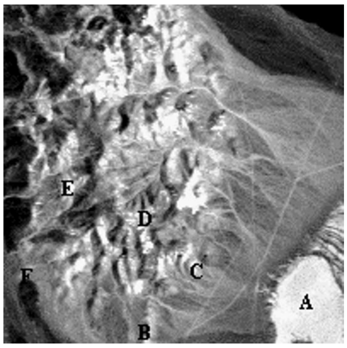

Fig. 1. A subsection of the Cuprite scene. The upper-case letters denote the positions of the pure materials found. The letter “A” stands for playa, “B” for kaolinite, “C” for alunite, “D” for silica, “E” for buddingtonite, and “F” for varnished tuff.

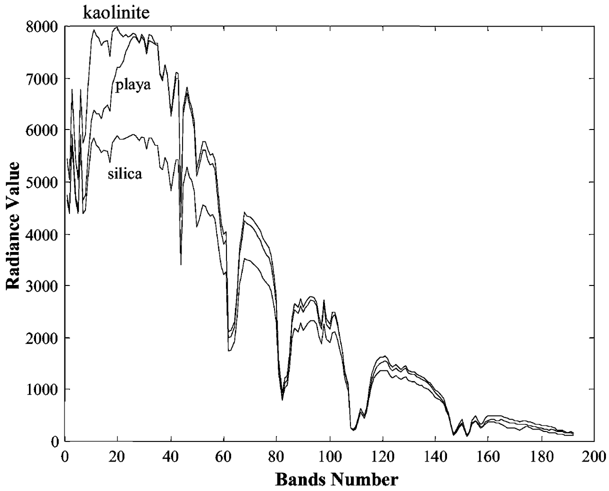

Fig. 2. Endmember radiance spectra in Simulation 1.

playa, kaolinite, and silica.

In the simulation experiment, a simulated 50×50 pixel scene was produced with three endmembers: playa, kaolinite, and silica. Each pixel in the simulated scene randomly contained a distinct abundance of endmembers forming the signal covariance matrix $\boldsymbol{R}_s$. That is, a simulated pixel could be $x\%$ kaolinite, $y\%$ playa, and $z\%$ silica with $x + y + z = 100$. The noise covariance matrix $\boldsymbol{R}_n$ was directly estimated from the water region in the original Cuprite image. $\boldsymbol{R}_s + \boldsymbol{R}_n$ represents the covariance matrix $\boldsymbol{R}$ of this simulation experiment. Figure 3 summarizes the simulation results. Although a total of 192 eigenvalues were obtained in the experiment, this figure and

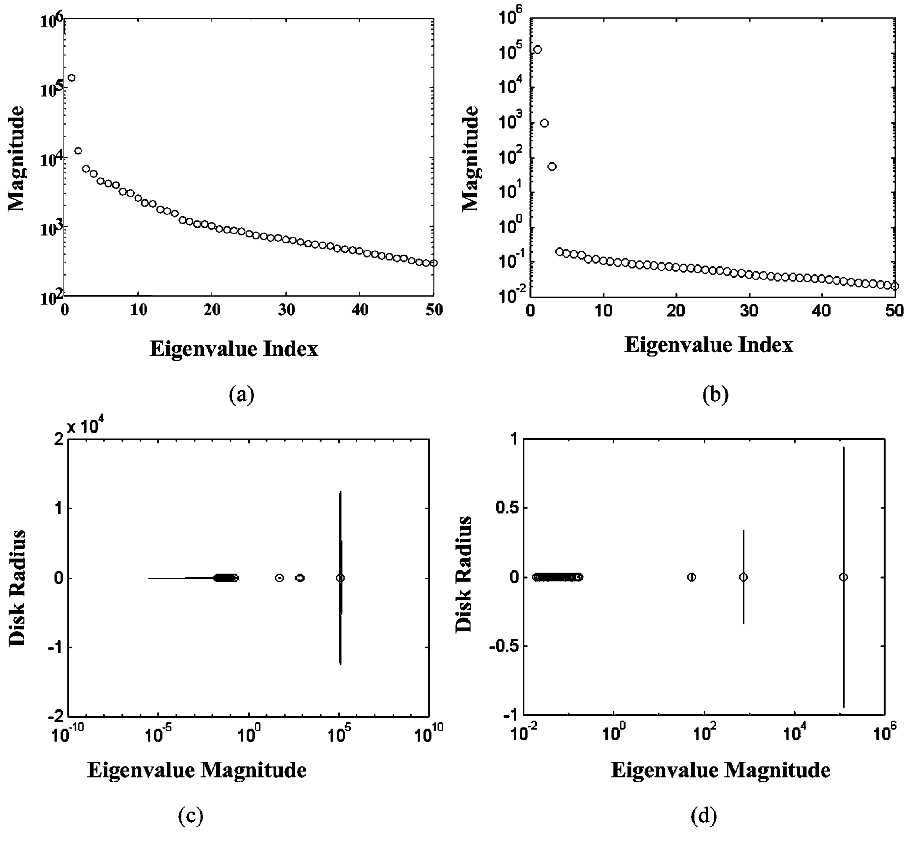

Fig. 3. Simulation 1 results for the four techniques. (a) PCA, (b) NAPCA, (c) MTGD and (d) the proposed VD transform. Only the first 50 eigenvalues are plotted for clarity.

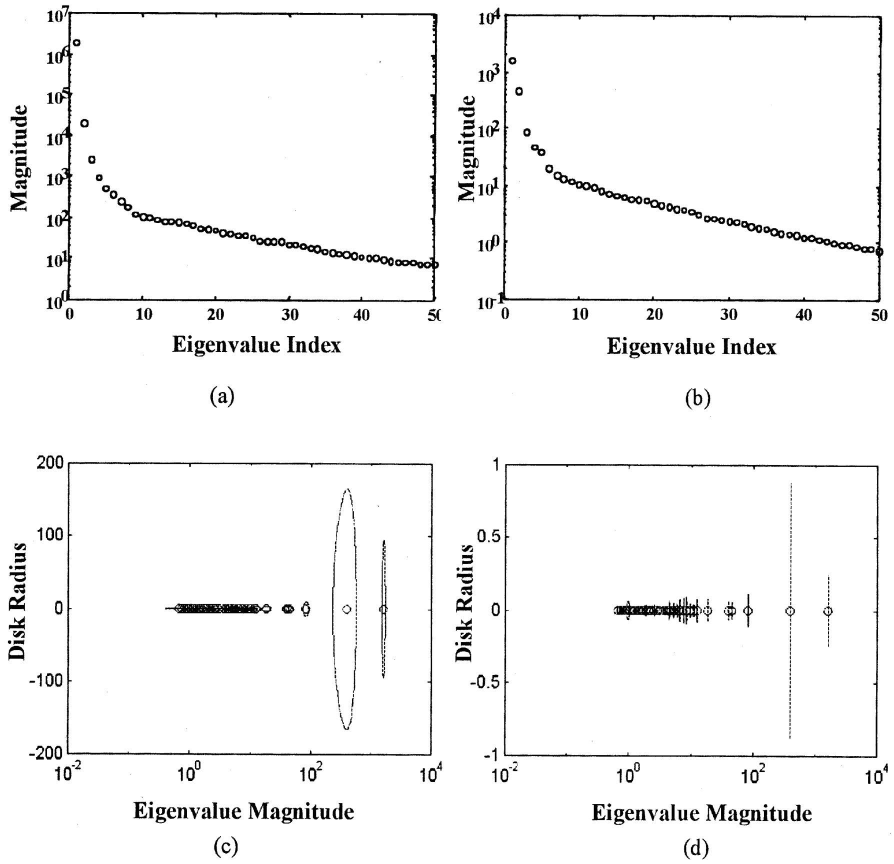

Fig. 4. Actual detection results for the four techniques. (a) PCA, (b) NAPCA, (c) MTGD, and (d) VD.

the remaining experimental results only include the first fifty eigenvalues for clarity. Results obtained from PCA and shown in Fig. 3(a) provide clear identification of only the first two signal eigenvalues. Figure 3(b) displays the NAPCA results. According to this figure, all the small eigenvalues are from noise while the other large eigenvalues were from the signal. The gap between large and small eigenvalues shown in this figure is obvious, so three endmembers were found by NAPCA. Figure 3(c) summarizes the results the MTGD transform. The centers and radii of the disks shown in this figure originated from eigenvalues and corresponding transformed covariances, respectively. The MTGD transform is advantageous in that all separated large disks denote signals while connected small disks denote noises. Although the resemble ellipses or lines due to the different scales for the x- and y-axis, all the “disks” displayed in the related figures derived using both the MTGD and VD methods are actually circles. According to our results, three endmembers were found, as shown in Fig. 3(c). The VD transform utilizes correlation values as the radii of disks to produce clearer separation than MTGD can. Figure 3(d) shows that although three endmembers could also be found, a better visual effect, i.e., disks kept farther away than in the case of MTGD, was obtained using VD.

Next, these four techniques were directly applied to the subsection of the actual detected Cuprite image. Figure 4 summarizes those results. Figure 4(a) shows the PCA results. It is obviously an overestimate. According to Fig. 4(b), only the first five eigenvalues produced by NAPCA could be clearly separated while the gap between other consecutive signals and noise eigenvalues was inadequately large. Figure 4(c) and (d) summarize the MTGD and VD results, respectively. Although the sixth disk shown in Fig. 4(c) can be regarded as a signal disk, there appears to be a slight connection with the noise disks. On the contrary, the result obtained using VD displays the separation clearly. Therefore, the VD method is the optimum scheme for solving the intrinsic dimensionality problem.

Experiment 2. The experiments in the second example involved a subsection of the LCVF image, which is also a 200×200 pixel scene. Figure 5 illustrates the 0.752 μm band of the image. This scene contains 158 bands in this study. This area has also been studied extensively using field measurements (Farrand, 1991), and the area has been modeled previously using spectral mixture analysis (Farrand, 1991; Harsanyi and Chang, 1994). The upper-case letters denote

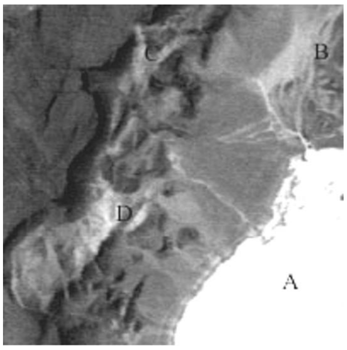

Fig. 5. A subsection of the LCVF scene. The upper-case letters denote the positions of the pure materials found. The letter "A" satnds for dry playa lakebed, "B" for vegetation, "C" for red oxidized basaltic cinders, and "D" for rhyolite.

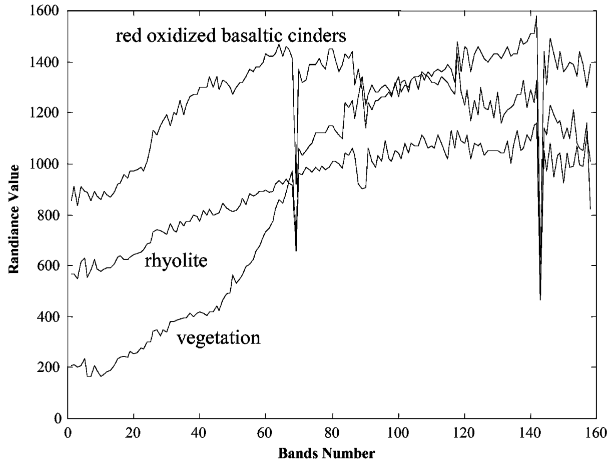

Fig. 6. Endmenber radiance spectra in Simulation 2.

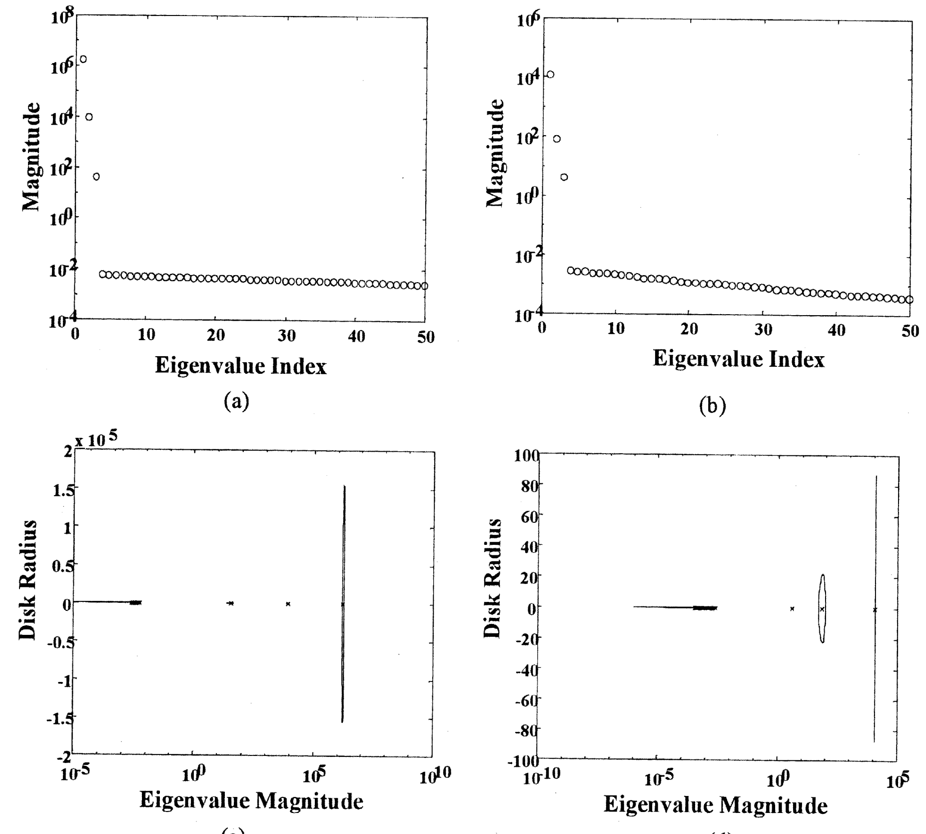

Fig. 7. Simulation 1 results for the four techniques. (a) PCA, (b) NAPCA, (c) MTGD, and (d) VD.

the positions of the pure materials found, which contained four significant materials: dry playa lakebed, vegetation, red oxidized basaltic cinders, and rhyolite.

In the simulated part, vegetation, red oxidized basaltic cinders, and rhyolite were used as the endmembers for a simulated 50×50 pixel scene. Figure 6 depicts the radiance spectra for these three materials. The procedure for generating simulated pixels for this experiment was the same as that adopted in Experiment 1. However, $\boldsymbol{R}_n$ was directly estimated from the homogenous region of the dry playa lakebed herein. Figure 7 summarizes the simulation results obtained using these four methods. According to this figure, all four techniques could accurately estimate the number of simulated

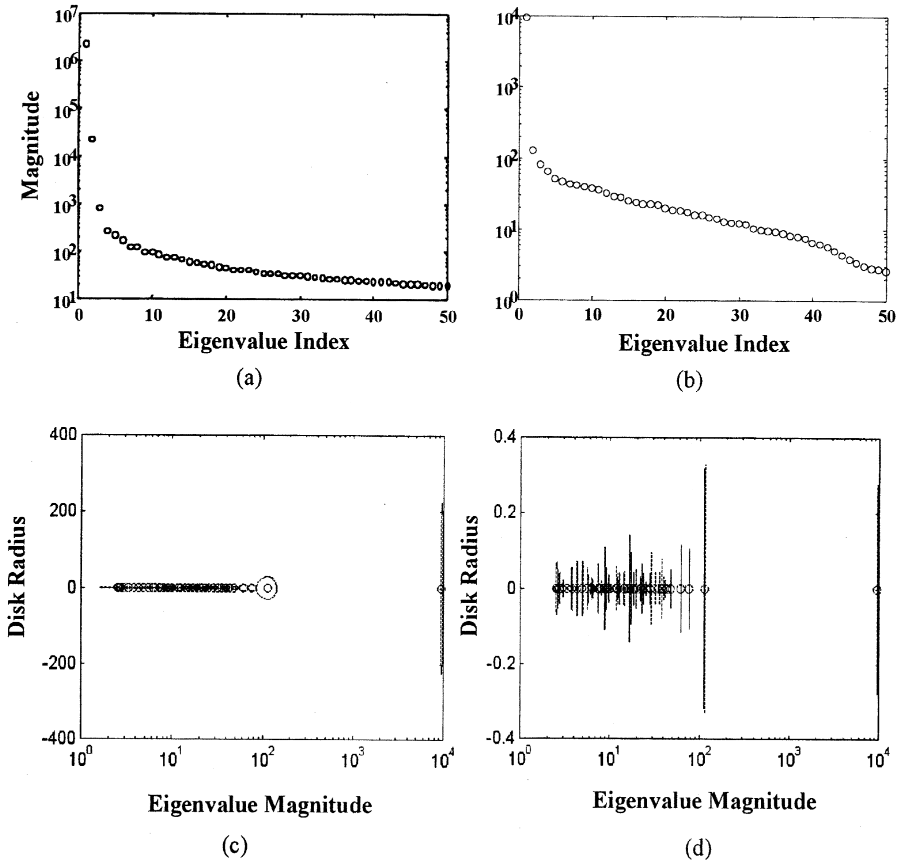

Fig. 8. Actual detection results for the three techniques. (a) PCA, (b) NAPCA, (c) MTGD, and (d) VD.

endmembers.

Again, these four techniques were directly applied to the subsection of the LCVF image. Figure 8 displays the results. Results obtained using PCA and shown in Fig. 8(a) provide clearly indicate only the first three signal eigenvalues. As for the NAPCA results shown in Fig. 8(b), although the largest two signal eigenvalues could be clearly separated, the next two were close to the noise eigenvalues. Hence, the performance of NAPCA in determining the intrinsic dimensionality was not satisfactory. Figure 8(c) reveals that although MTGD produced four larger disks for signals, they were connected to the noise disks except for the first (largest) one. The VD results shown in Fig. 8(d) reveal four signal disks clearly since their radii are small enough. Moreover, the fifth signal disk can be seen in Fig. 8(d) although it appears to be loosely overlapping the noise disks. If we enlarge the scale of the x-axis in Fig. 8(c) and (d), the distribution of the first ten eigenvalues can be displayed, as it is in Fig. 9(a) and (b). Obviously, the fifth signal disk shown in Fig. 9(a) slightly overlaps the collection of noise disks, but could be separated from noise disks as shown in Fig. 9(b). This finding suggests that previous modeling efforts could have been improved by considering an additional endmember in the spectral mixture analysis. Information of the fifth eigenvalue indicates that

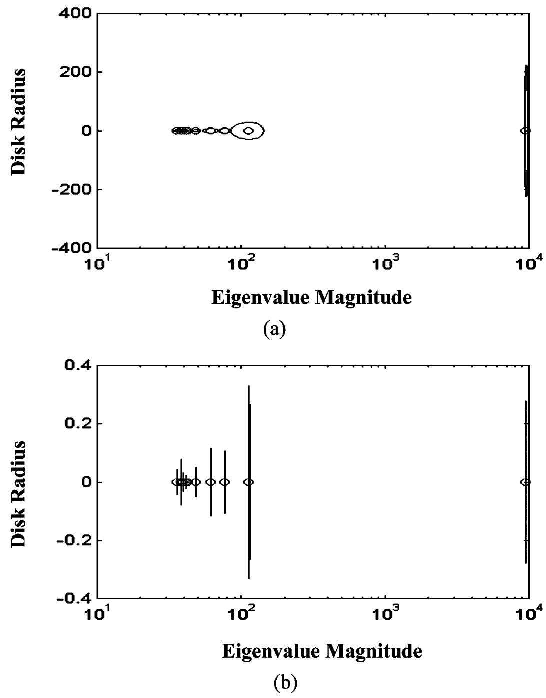

Fig. 9. An enlarged version of Fig. 8(c) and (d), which display only the first ten eigenvalues.

extra material with a low probability of occurrence exists within the scene. This material may be only present in a small number of pixels or mixed pixels. This finding closely corresponds to our earlier work (Tu *et al.*, 1998), which used a noise subspace projection (NSP) approach to perform target signature detection in this scene.

VI. Conclusion

This work has presented two novel approaches to determining the intrinsic dimensionality, or equivalently, the number of image endmembers in a hyperspectral data cube. The first approach is a modified version of the MTGD, which incorporates NAPCA into a TGD approach and retains the merits of both NAPCA and TGD simultaneously. The second method, referred to as the VD method, is based on multiple linear regression. In addition, a novel transform kernel has been derived to upgrade the estimation ability and visualization effect of MTGD. The subsequent Gerschgorin disks in VD can be formed into two more distinct signal and noise collections compared to both TGD and MTGD. Experimental results indicate that VD not only performs better than NAPCA and MTGD in computer simulations, but also operates effectively with AVIRIS data, whereas NAPCA and MTGD appear to underestimate the number of endmembers in a low SNR situation.

Acknowledgment

The authors would like to thank the National Science Council of the Republic of China for financially supporting this work under contract NSC 87-2213-E-014-005. We thank Professor Chein-I Chang of the University of Maryland, Baltimore, and Dr. J. C. Harsanyi for providing the AVIRIS data of the Lunar Crater Volcanic Field. We also thank NASA-JPL for providing the AVIRIS data of Cuprite, Nevada. The authors also extend thanks to Dr. Hsien-Tsai Wu for many valuable comments on the transformed Gerschgorin disk method.

References

Adams, B. and M. O. Smith (1986) Spectral mixture modeling: a new analysis of rock and soil types at the Viking Lander 1 site. *J. Geophys. Res.*, **91**, 8098-8112.

Akaike, H. (1974) A new look at the statistical model identification. *IEEE Trans. Automatic Control*, **19**(6), 716-723.

Alan, J. (1977) *Matrix Computation for Engineers and Scientists*. John Wiley & Sons, New York, NY, U.S.A.

Anderson, T. W. (1984) *An Introduction to Multivariate Statistical Analysis*. John Wiley & Sons, New York, NY, U.S.A.

Research Systems Inc. (1997) *ENVI User's Guide*, Version 2.6. Boulder, CO, U.S.A.

Farrand, W. H. (1991) Analysis of Altered Volcanic Pyroclasts using AVIRIS data. *Proceedings of the Third AVIRIS Workshop*, JPL Publication 91-28, JPL, NASA, Washington, D.C., U.S.A.

Fukanaga, K. (1990) *Introduction to Statistical Pattern Recognition*, 2nd Ed. Academic Press, New York, NY, U.S.A.

Green, A. A., M. Berman, P. Switzer, and M. Craig (1988) A transformation for ordering multispectral data in terms of image quality with implications for noise removal. *IEEE Trans. Geos. Remote Sensing*, **26**(1), 65-74.

Harsanyi, C. and C. I. Chang (1994) Hyperspectral image classification and dimensionality reduction: an orthogonal subspace projection approach. *IEEE Trans. Geos. Remote Sensing*, **32**(4), 779-785.

Lee, J. B., A. S. Woodyatt, and M. Berman (1990) Enhancement of high spectral resolution remote sensing data by a noise-adjusted principal components transform. *IEEE Trans. Geos. Remote Sensing*, **28**, 295-304.

Rissanen, J. (1978) Modeling by shortest data description. *Automatica*, **14**, 465-471.

Roger, R. E. (1990) A fast way to compute the noise-adjusted principal components transform matrix. *IEEE Trans. Geos. Remote Sensing*, **32**, 1194-1196.

Swayze, G. A., R. N. Clark, S. Sutley, and A. Gallagher (1992) Ground-truthing AVIRIS mineral mapping at Cuprite, Nevada. *Summaries of the Third Annual JPL Airborne Geosciences Workshop, Volume 1: AVIRIS Workshop*, JPL Publication 92-14, JPL, NASA, Washington, D.C., U.S.A.

Tu, T. M., C. H. Chen, and C. I. Chang (1998) A noise subspace projection approach to target signature detection and extraction in unknown background for hyperspectral images. *IEEE Trans. Geos. Remote Sensing*, **36**(1), 171-181.

Vane, G. and A. F. H. Goetz (1988) Terrestrial imaging spectroscopy. *Remote Sensing Environs*., **24**(1), 1-29.

Wax, M. and T. Kailath (1985) Detection of signals by information theoretic criteria. *IEEE Trans. Acoustics, Speech, Signal Processing*, **33**(2), 387-392.

Wu, H. T., J. F. Yang, and F. K. Chen (1995) Source number estimation using transformed Gerschgorin radii. *IEEE Trans. on Signal Processing*, **43**, 1325-1333.

A Visual Disk Approach

應用一個視碟法來決定超高維影像的本質維度

杜德銘[*]　李靖海[*]　江中熙[*]　張劍平[**]

[*]中正理工學院電機工程學系
[**]中山科學研究院

摘　要

在衛星遙測影像的分析中，對於地物的種類及其分布量的判釋一直是相當重要的一環；然而在未知背景的環境下，我們必須先探勘出觀測環境中所含的地物數量，才能作爲進一步處理的依據。理論上，探勘地物的數量與決定影像的本質維度是相同的問題。在過去，雜訊調整主值分析法一直是探勘地物數量的一項重要工具；然而，它在實用時必須先準確地估測出所要分析影像的雜訊模式，才能得到正確的結果；如果雜訊模式估測不準確，本質維度也就無法正確的估測。爲了解決這個問題，本文中我們提出了一個新的視碟法，結合了雜訊調整主值分析法與轉換高須哥令碟法，並利用多重線性迴歸將代表訊號與雜訊次空間的高須哥令碟分隔成二個不會重疊的部分；如此我們僅需計數訊號次空間的碟數，即可找出所要分析影像的本質維度。根據視碟法應用在AVIRIS影像的實驗結果顯示，視碟法的確是一個估測影像本質維度的好方法。